

# Searching for cluster substructure using APM and ROSAT data.

V. Kolokotronis<sup>1</sup>, S. Basilakos<sup>2,1,3</sup>, M. Plionis<sup>1</sup>, I. Georgantopoulos<sup>1</sup>.

<sup>1</sup> *Institute of Astronomy & Astrophysics, National Observatory of Athens, Lofos Nimfon, Thessio, 18110 Athens, Greece*

<sup>2</sup> *Astrophysics Group, Imperial College London, Blackett Laboratory, Prince Consort Road, London SW7 2BW, UK*

<sup>3</sup> *Physics Department, University of Athens, Panepistimiopolis, Greece*

28 October 2018

## ABSTRACT

We present a detailed study of the morphological features of 22 rich galaxy clusters. Our sample is constructed from a cross-correlation of optical (Abell+APM) data with X-ray (0.1 - 2.4) keV ROSAT pointed observations. We systematically compare cluster images and morphological parameters in an attempt to reliably identify possible substructure in both optical and the X-ray images. To this end, we compute various moments of the optical and X-ray surface-brightness distribution such as the ellipticities, center-of-mass shifts and ellipsoidal orientations. We assess the significance of our results using Monte Carlo simulations. We find significant correlations between the optical and X-ray morphological parameters, indicating that in both parts of the spectrum it is possible to identify correctly the dynamical state of a cluster. Most of our clusters (17/22) have a good 1-to-1 correspondence between the optical and the X-ray images and about 10 appear to have strong indications of substructure. This corresponds to a minimum percentage of order  $\sim 45\%$ , which is in very good accordance with other similar analyses. Finally, 5 out of 22 systems ( $\sim 22\%$ ) seem to have distinct subclumps in the optical which are not verified in the X-ray images, and thus are suspect of being due to optical projection effects. These results will serve as a useful guide in interpreting subsequent analyses of large optical cluster catalogues.

**Keywords:** galaxies: clusters: general - large-scale structure of universe - X-ray: galaxy clusters

## 1 INTRODUCTION

Galaxy clusters occupy a special position in the hierarchy of cosmic structure in many respects. Being the largest physical laboratories in the universe, they appear to be ideal tools for studying large-scale structure, testing theories of structure formation and extracting invaluable cosmological information, especially regarding the Hubble parameter and the value of  $\Omega_0$  (cf. Böhringer 1995; West, Jones & Forman 1995; Buote 1998; Schindler 1999).

One of the most significant properties of galaxy clusters is the relation between their dynamical state and the underlying cosmology. In an open universe, clustering effectively freezes at high redshifts ( $z \simeq \Omega_0^{-1} - 1$ ) and clusters today should be more relaxed with weak or no indications of substructure. Instead, in a critical den-

sity model, such systems continue to form even today and should appear to be dynamically active. Even, in a small but well-controlled (from any kind of selection or other biases) cluster sample, the percentage and morphologies of disordered and perturbed objects could lead to constraints on the  $\Omega_0$  and  $\Lambda$  parameters, especially if combined with N-body/gasdynamical numerical simulations spanning different dark matter (DM) scenarios (cf. Richstone, Loeb & Turner 1992 hereafter RLT92; Evrard et al. 1993; Lacey & Cole 1993).

The above pioneering works were the first to set some limits on  $\Omega_0$  using the rate of cluster formation for various cosmologies and led the way to a plethora of research works towards this direction (see Figure 2 of RLT92). Since then, a large number of relevant analyses have been devoted to this study and an accordingly varying and large number of optical and X-ray clus-

ter compilations have been utilised to this aim. All the methods employed in each case are quite different and all the related studies find an appreciable percentage of dynamically active galaxy clusters (see Forman & Jones 1990; Böhringer 1995; West 1995; Thomas et al. 1998 for good reviews of the subject). However, these studies do disagree on the precise number of clusters exhibiting significant dynamical activity, which varies between 30% and 80% of the total number of clusters studied, and which seems also to depend on the techniques employed in each analysis.

We quote only some of the most recent studies together with the sample used and the preference of the method given in each case. Geller & Beers (1982) analysed the iso-intensity contour maps of 65 optical clusters maps. Forman et al. (1981) studied 4 Einstein clusters. Dressler & Shectman (1988) studied velocity dispersion diagnostics for 15 optical clusters. Rhee, van Haarlem & Katgert (1991) and Solanes, Salvador-Sole & Gonzalez-Casado (1999) utilised 107 and 67 ENACS clusters respectively and a variety of 2D and 3D statistical tests to quantify the significance of substructure. Similarly, Dutta (1995), Crone, Evrard & Richstone (1996 hereafter CER96), Pinkney et al. (1996), Thomas et al. (1998 hereafter T98) and Jones & Forman (1999 hereafter JF99; 208 ROSAT X-ray clusters) proposed a variety of substructure tests depending on the level of information available (1D, 2D, 3D) and applied these to different N-body cluster data using several DM models. CER96 and T98 have explicitly argued that variations in the cluster center-of-mass as a function of distance or density (overdensity) threshold is one of the best possible substructure measures (see also West & Bothun 1990). The latter has previously been adopted by Mohr, Fabricant & Geller (1993; 5 X-ray clusters), Mohr et al. (1995; 65 Einstein clusters) and Rizza et al. (1998; 11 ROSAT HRI distant clusters). Evrard et al. (1993) and Mohr et al. (1993; 1995) were the first to make extensive use of the surface-brightness moments of the X-ray cluster distribution (eg. center-of-mass shifts). Gomez et al. (1997; 9 Abell clusters) have also employed the same methods and claimed that variations in the cluster ellipticity and orientation as a function of distance from the cluster center (isophotal twisting) should be considered as one of the prime substructure diagnostics. Bird (1994) in her sample of 25 Abell cluster has utilised galaxy peculiar velocities to locate and identify subclumps in the galaxy distribution. Kriessler & Beers (1997; 56 Abell and other clusters) have searched for cluster substructure signatures using the innovative KMM algorithm on the surface-density galaxy maps and quantified their findings using N-body simulations. Furthermore, Buote & Tsai (1995; 1996 hereafter BT95; BT96) and Valdarnini, Ghizzardi & Bonometto (1999) used the 2D gravitational potential moments (power ratio method) to characterise the

dynamical state of clusters. Serna & Gerbal (1996; 2 Abell clusters) have developed the so-called hierarchical method to define and identify substructure in Abell clusters, while Slezak et al. (1994; 11 X-ray clusters) and Lazzati et al. (1998; 2 X-ray clusters) have adopted wavelet transform techniques in similar attempts.

As it is evident from all the above there is neither agreement on the methods utilised nor on the exact frequency of perturbed clusters. It seems that identifying significant dynamical activity within galaxy clusters, in close relation to the underlying cosmology and the density parameter, still remains an open issue. Not only do we need a large, statistically complete, cluster sample but an objective and reliable definition of what substructure is, upon which our study should be based.

The large majority of the analyses carried out so far, have made use of either optical (Abell) or X-ray (ROSAT, Einstein) cluster data. However, Mohr et al. (1993) and Rizza et al. (1998) have investigated cluster substructure using in a complementary fashion optical and X-ray data. In the present work, we extend this approach using a sample of 22 galaxy clusters for which we have data both in the optical and the X-ray part of the spectrum (APM and ROSAT respectively). Our sample size is twice as large as that of Rizza et al. (1998) and more than four times larger than that of Mohr et al. (1993). The advantage of using X-ray data is that the X-ray emission is proportional to the square of the gas density (rather than just density in the optical) and emanates mostly from the central cluster region, a fact which minimises projection effects (cf. Sarazin 1988; Schindler 1998). The advantage of using optical data is the sheer size of the available cluster catalogues and thus the statistical significance of the emanating results. Subsequently, we are not only interested in comparing optical to X-ray cluster data regarding the various substructure tools, but to calculate and calibrate different biases using the superior X-ray data with which we could measure and test easily similar substructure diagnostics in a large, solely optical dataset as well. Therefore it is of great importance to address the following two questions, which we attempt to do in our present study:

- Is substructure in the optical also corroborated by the X-ray observations and in what percentage?
- What is the confirmed percentage of systems depicting significant indications of internal activity?

To this aim we compare optical to X-ray morphological cluster parameters (position angles, ellipticities, centroid shifts and group statistics) in an attempt to classify objects according to their dynamical state and we compute the relative frequency of substructure.

We proceed by presenting the optical and X-ray datasets in section 2. In section 3, we describe our methods of analysis, in section 4 we present a comparison of

the optical and X-ray cluster images while in section 5 we present the results of our substructure analysis. Finally, we draw our conclusions in section 6. Also, there is an extensive appendix at the end of this paper, where morphological and dynamical information for each individual cluster can be found as well as a comparison with other similar works on the common clusters.

## 2 THE DATA

The present dataset follows from a double cross-correlation between very rich ACO (Abell, Corwin & Olowin 1989) clusters ( $R \geq 1,2,3$ ) with the APM cluster catalogue (Dalton et al. 1997 and references therein) and the X-ray (0.1 - 2.4) keV ROSAT pointed observations archive. The first correlation results in 329 common optical galaxy clusters (ACO/APM) in the southern sky ( $b \leq 40^\circ, \delta \leq -17^\circ$ ), while the second correlation results in 27 common clusters. Due to problematic regions of the APM catalogue, low signal to noise X-ray observations, contamination by known foreground or background objects and even double entries we exclude 5 clusters (A4038, A122, A3264, A3049 and A2462) reducing our cluster sample to 22 systems.

Furthermore, the ROSAT (Trümper 1983) data we have used come from both the PSPC (Positional Sensitive Proportional Counter; Pfefferman & Briel 1986), and the HRI (High Resolution Imager) detectors, both operating in the (0.1 - 2.4) keV band. The HRI has an excellent spatial resolution (FWHM  $\sim 5$  arcsec) but no spectral resolution. The PSPC has an energy resolution of 0.5 keV at 1 keV but poorer spatial resolution (30 arcsec FWHM) compared to HRI. We note that the PSPC is quite efficient in detecting extended emission, in contrast with the HRI which has a lower sensitivity due to its higher background.

The cluster redshifts of our sample span the range  $0.04 \lesssim z \lesssim 0.13$  with  $\langle z \rangle \sim 0.074$  and median  $\sim 0.069$ . For the needs of our analysis we transform cluster redshifts to cluster distances using the well-known angular-diameter distance formula with  $q_0 = 0.5$  (ie., critical density universe) as:

$$r = \frac{2c}{H_0} (1+z)^{-1/2} [1 - (1+z)^{-1/2}] , \quad (1)$$

with  $H_0 = 100 h \text{ km s}^{-1} \text{ Mpc}^{-1}$ . In Table 1 we give all the relevant details for the present cluster sample.

## 3 THE METHODOLOGY

In this section we provide an account of the techniques used to define the cluster morphological parameters as well as the substructure measures. We first present how to *process* the cluster images and reduce the noise from point-like sources.

**Table 1.** Details of our cluster sample: APM and ACO index numbers, equatorial coordinates (1950) of cluster centers in degrees, heliocentric redshift, richness class, type of ROSAT observation and exposure time (in seconds). All cluster redshifts are taken from Katgert et al. (1996) and Mazurek et al. (1996), apart from those of A2804 (Dalton et al. 1994), A2811 (Collins et al. 1995) and A2580 (White, Jones & Forman 1997). For A3144 and A2580 we have used  $m_{10}$  estimated redshifts.

| APM | ACO  | $\alpha$ | $\delta$ | $z$    | R | Type | $t_{\text{exp}}$ |
|-----|------|----------|----------|--------|---|------|------------------|
| 5   | 2717 | 0.1083   | -36.3113 | 0.0498 | 1 | PSPC | 10000            |
| 15  | 2734 | 2.1783   | -29.1011 | 0.0620 | 1 | PSPC | 5000             |
| 99  | 2804 | 9.2962   | -29.1639 | 0.1080 | 1 | PSPC | 7500             |
| 104 | 2811 | 9.9729   | -28.8475 | 0.1090 | 1 | HRI  | 9350             |
| 138 | 0133 | 15.0516  | -22.2228 | 0.0570 | 1 | HRI  | 12500            |
| 204 | 2933 | 24.6966  | -54.8097 | 0.0930 | 1 | PSPC | 7900             |
| 347 | 3093 | 47.4212  | -47.6186 | 0.0830 | 2 | PSPC | 8100             |
| 373 | 3111 | 49.0317  | -45.8886 | 0.0780 | 1 | PSPC | 7600             |
| 374 | 3112 | 49.0337  | -44.4247 | 0.0750 | 2 | HRI  | 9600             |
| 403 | 3128 | 52.2929  | -52.7231 | 0.0600 | 3 | HRI  | 6500             |
| 427 | 3144 | 54.0304  | -55.2681 | 0.0450 | 1 | PSPC | 2921             |
| 434 | 3158 | 55.3371  | -53.7884 | 0.0590 | 2 | PSPC | 3050             |
| 484 | 3223 | 61.5212  | -31.0419 | 0.0601 | 2 | PSPC | 7700             |
| 510 | 3266 | 67.6329  | -61.5120 | 0.0589 | 2 | HRI  | 8202             |
| 518 | 0500 | 69.1946  | -22.1964 | 0.0670 | 1 | PSPC | 18400            |
| 533 | 0514 | 71.5001  | -20.5692 | 0.0730 | 1 | PSPC | 18105            |
| 560 | 3301 | 74.8496  | -38.8044 | 0.0540 | 3 | PSPC | 8886             |
| 725 | 2384 | 327.385  | -19.8139 | 0.0943 | 1 | HRI  | 26144            |
| 806 | 3897 | 339.129  | -17.6010 | 0.0733 | 1 | PSPC | 4300             |
| 822 | 3921 | 341.5895 | -64.6525 | 0.0940 | 2 | PSPC | 12000            |
| 888 | 2580 | 349.6854 | -23.4619 | 0.1297 | 1 | HRI  | 17663            |
| 938 | 4059 | 358.6346 | -34.8300 | 0.0488 | 1 | HRI  | 6320             |

### 3.1 Processing the cluster images

Our X-ray cluster images are retrieved from the ROSAT pointed observations archive and we have used the image processing package XIMAGE, which is designed to display and reduce the available data. Each X-ray image is embedded in a  $512 \times 512$  grid, each cell of which has a size of 15 arcseconds. We subtract all known point-like sources around the clusters (cf. West 1995; JF99) and replace them with the average background counts. In doing so, we have mostly encountered radio point-like sources (see Appendix for details).

Our optical data consist of all APM galaxies that fall within a radius of  $1.8 h^{-1} \text{ Mpc}$  from each optical APM cluster center. We then transform the galaxy and X-ray grid-cell angular coordinates into physical units, centering the X-ray data on the optical cluster centers. In order to construct a common comparison base, we create a continuous density field for both optical and X-ray data by using a Gaussian Kernel and the same smoothing length ( $R_{\text{sm}}$ ). To this end we utilise a  $N \times N$  grid, where the typical size of each grid cell is  $\sim 0.065 h^{-1} \text{ Mpc}$ . In order to take into account the reduction of the number of galaxy cluster members as a function of distance (due to the APM magnitude limit), and thus the corresponding increase of discreteness ef-

fects, we have investigated, using Monte-Carlo cluster simulations, the necessary increase in size of  $N$  and  $R_{\text{sm}}$ , as a function of distance, in order to minimise such effects and optimize the performance of our procedure (for details see Basilakos, Plionis & Maddox 2000; hereafter BPM).

### 3.2 Cluster Shape Parameters

We compute the optical and X-ray cluster shape parameters utilising the method of moments of inertia (cf. Carter & Metcalfe 1980; Plionis, Barrow & Frenk 1991; BPM). We can then write the moments as follows:

$$I_{11} = \sum_{i=1}^N \rho_i (r_i^2 - x_i^2) \quad (2)$$

$$I_{22} = \sum_{i=1}^N \rho_i (r_i^2 - y_i^2) \quad (3)$$

$$I_{12} = I_{21} = - \sum_{i=1}^N \rho_i x_i y_i, \quad (4)$$

where  $\rho_i$  is the cell density,  $x_i, y_i$  are the Cartesian coordinates of the grid cells and  $r_i = \sqrt{x_i^2 + y_i^2}$ . If we now diagonalise the inertia tensor  $\det(I_{ij} - \lambda^2 M_2) = 0$  ( $M_2$  being the  $2 \times 2$  unit matrix), we can obtain the eigenvalues  $\lambda_1, \lambda_2$ , from which the ellipticity of each object can be estimated as  $\epsilon = 1 - \lambda_2/\lambda_1$ , with  $\lambda_1 > \lambda_2$ . The eigenvectors, corresponding to these eigenvalues, provide us with the cluster orientations. The major axis orientation with respect to the North, in the anticlockwise direction, is the so-called cluster position angle ( $\theta$  hereafter).

The shape parameters are estimated using all cells that have densities above three thresholds. These are defined as the average density of all cells that fall within a chosen radius. The three radii used are  $r_\rho = 0.3, 0.45$  and  $0.6 h^{-1}$  Mpc. The choice of such a step size is not arbitrary, however. We have tested the robustness of our procedure using different step sizes, ranging from  $\sim 0.1 h^{-1}$  Mpc to  $\sim 0.3 h^{-1}$  Mpc to find that the former is too small, since it will only locate the highest density peaks in the galaxy or hot gas distribution, while the latter is somewhat too large since it typically registers very low density fluctuations, comparable to the background level of the cluster image. The above spatially defined procedure overcomes the difficulty of determining the density thresholds in the two intrinsically different (optical and X-ray) density distribution.

Note that for each cluster we find the highest cluster density-peak ( $x_p, y_p$ ) within a radius of  $\sim 0.5 h^{-1}$  Mpc around the original APM cluster center. We then redefine the cluster center as being ( $x_p, y_p$ ) and estimate all shape parameters around this new coordinate center. Typically, this coincides with the registered APM cluster center. We can get an idea of the regions of the

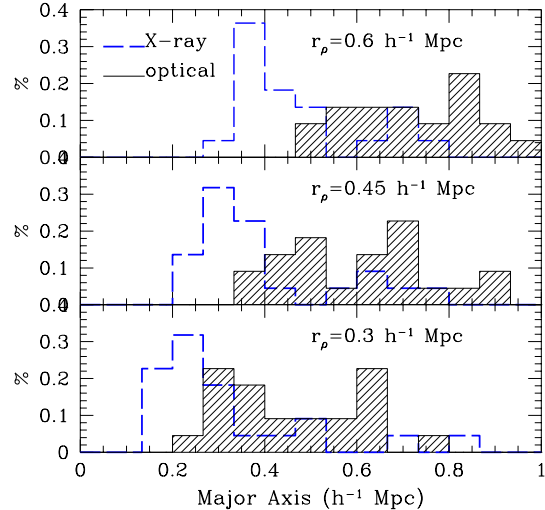


**Figure 1.** Distribution of major axes of the fitted ellipses for the optical (hatched) and X-ray cluster images and for the three density thresholds based on the indicated  $r_\rho$  (see definition in the text).

clusters sampled by our procedure by inspecting Figure 1 where we plot the resulting major axis of the fitted ellipses in each distribution and for the three density thresholds. It is evident that the regions sampled in the X-ray images are more centrally concentrated, as expected.

### 3.3 Substructure Measures

#### 3.3.1 Ellipticity

It is expected that the existence of significant substructure affects the shape of the cluster in the direction of producing large ellipticities (McMillan et al. 1989; Davis & Mushotzky 1993; West et al. 1995; Gomez et al. 1997). Although this appears to be a robust prediction, a small  $\epsilon$  does not always endorse the lack of substructure. The reasons being that (a) small scale structure could develop symmetrically around the cluster core, and (b) a possible merger could happen along the line of sight. In both cases a small ellipticity would be measured.

#### 3.3.2 Cluster centroid shift

Evrard et al. (1993) and Mohr et al. (1993) have suggested as an indicator of cluster substructure the shift of the center-of-mass position as a function of density threshold above which it is estimated (see also CER96; T98). Following their suggestion, we define as *centroid-shift* ( $sc$ ) the distance between the cluster center-of-mass, ( $x_o, y_o$ ), where  $x_o = \sum x_i \rho_i / \sum \rho_i$ ,  $y_o = \sum y_i \rho_i / \sum \rho_i$  and the highest cluster density-peak, ie.,

$$sc = \sqrt{(x_o - x_p)^2 + (y_o - y_p)^2}. \quad (5)$$

Notice here, that while the cluster center-of-mass changes as a function of density threshold ( $\rho_t$ ), above which we define the cluster shape parameters, the position ( $x_p, y_p$ ) remains unchanged. A large value of  $sc$  may therefore furnish a first clear indication of substructure.

In order to quantify the significance of such centroid variations to the presence of background contamination and random density fluctuations, we carry out, in a fashion similar to BPM, a series of Monte Carlo cluster simulations in which we have, by construction, no substructure. For each cluster we produce a series of simulated clusters having the same number of observed galaxies as well as a random distribution of background galaxies, determined by the distance of the cluster and the APM selection function. Furthermore, the simulated galaxy distribution follows a King-like profile:

$$\Sigma(r) \propto \left[ 1 + \left( \frac{r}{r_c} \right)^2 \right]^{-\alpha}, \quad (6)$$

where  $r_c$  is the core radius,  $\alpha = (3\beta - 1)/2$  and  $\beta$  being the ratio of the specific energy in the galaxies to the specific thermal energy in the gas. We use the weighted, by the sample size, mean of most recent  $r_c$  and  $\alpha$  determinations (cf. Girardi et al. 1995; 1998), i.e.,  $r_c = 0.085 h^{-1}$  Mpc and  $\alpha = 0.7$ . We do test the robustness of our results for a plausible range of these parameters. In general we find that the significance of the  $sc$  measure decreases as  $r_c$  increases. This is to be expected since using a large value of  $r_c$ , for the same number of core galaxies, will increase the random density fluctuations and thus the  $sc$  measure. Naturally, we expect our simulated clusters to generate small  $sc$ 's and in any case insignificant shifts. Therefore, for each optical cluster in our sample we perform 1000 such simulations and we derive  $\langle sc \rangle_{\text{sim}}$  as a function of the same thresholds,  $\rho_t$ , as in the real cluster case. Then, within a search radius of  $0.75 h^{-1}$  Mpc from the simulated highest cluster peak, we calculate the quantity:

$$\sigma = \frac{\langle sc \rangle_o - \langle sc \rangle_{\text{sim}}}{\sigma_{\text{sim}}}, \quad (7)$$

in order to measure the significance of real centroid shifts as compared to those of relaxed, mock objects. Note that  $\langle sc \rangle_o$  is the average, over the three density thresholds, centroid shift for the real cluster.

### 3.3.3 Subgroup classes

We also utilise a friend-of-friends algorithm to categorise the observed substructure (see also section 3.2 of Rhee et al. 1991 for details). We join all cells having common boundaries that fall above each density threshold. We therefore create and register all subgroups as a function of  $\rho_t$  and rank substructure events according to the following 3 categories (see BPM and Plionis et al. 2000 *in preparation*):

- (1) *No substructure*: Clusters with only one group

at all density thresholds (regular, spherical systems). Systems with two unequal subgroups, where the second is much smaller than the first (*mincir*10%) also fall in this level.

- (2) *Weak or moderate substructure*: Objects with one clump at the first  $\rho_t$  and multiple clumps at the next two levels (second or third threshold), where the second in size group is greater than 10% and  $\lesssim$  25% of the total cluster size (see also RLT92).

- (3) *Strong substructure*: Like in (2) but now the second in size subgroup is  $\gtrsim$  25% of the total cluster size. Complex systems with multiple condensations at all density thresholds are naturally included in this category. Finally, a cluster with two large clumps (bimodal) at the highest density level, of which one is  $>$  40% of the other, fall in this category as well.

Note that in order to be consistent with the scale within which APM clusters are reliably identified and constructed (Dalton et al. 1997), we have used a radius of  $0.75 h^{-1}$  Mpc as our maximum searching radius within which we search for subgroup statistics. We have also carried out the same analysis by increasing the radius to  $1 h^{-1}$  Mpc but results do not change appreciably.

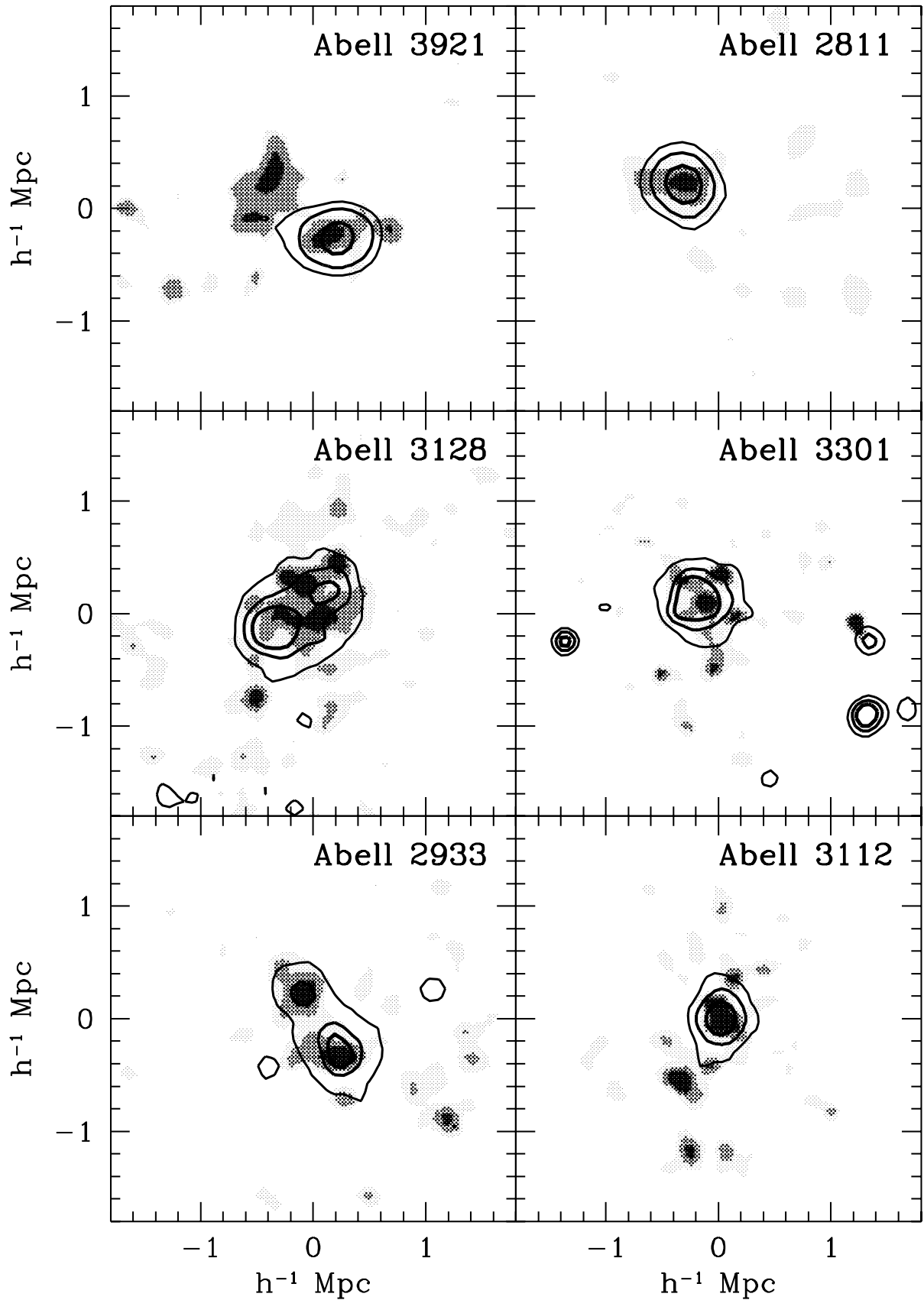
## 4 COMPARISON OF OPTICAL & X-RAY CLUSTER IMAGES

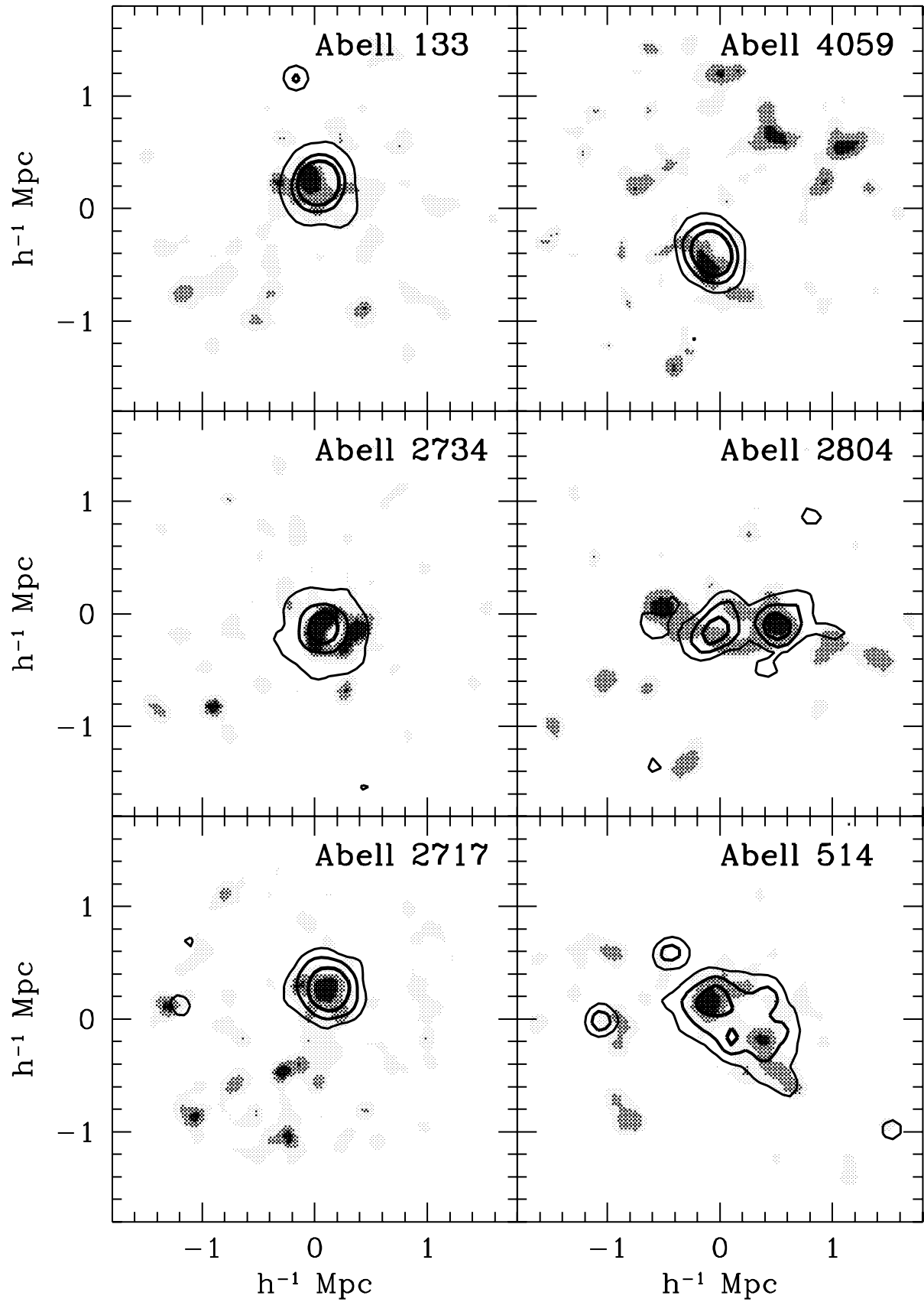
We investigate here the compatibility between the X-ray and optical cluster data by visually inspecting their smoothed density distributions as well as by correlating their respective shape parameters (ellipticity and position angles). The aim of our procedure is to evaluate how well the optical APM data trace the cluster potential and therefore how reliable the optical data can be in deriving the structural and dynamical parameters of clusters. This is of paramount importance since large cluster samples exist mostly in the optical and their analysis can provide important constraints in theories of galaxy formation.

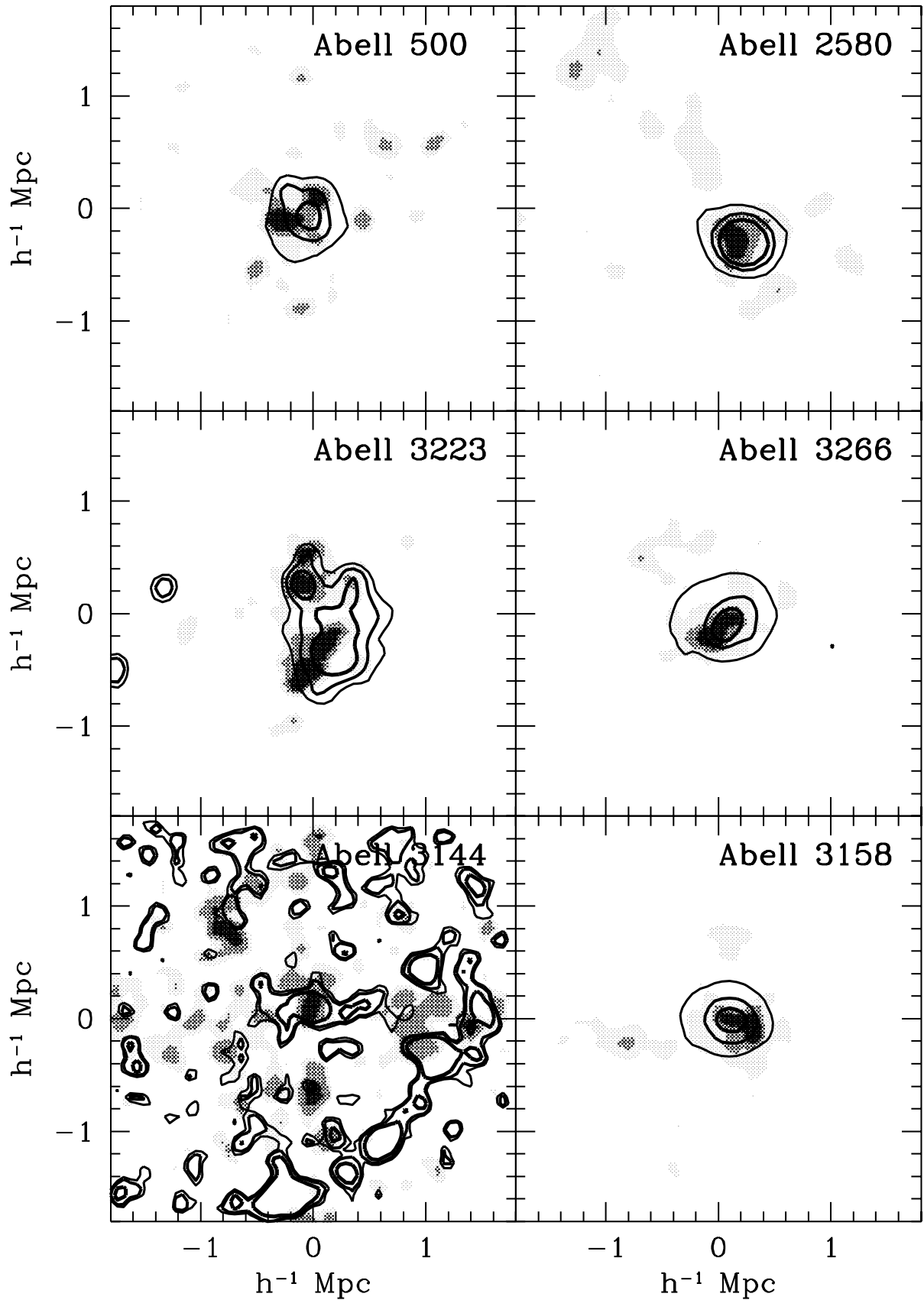
A similar comparison of optical and X-ray cluster data has been performed by Miller, Melott & Nichol (2000), and they found that optical total cluster luminosity is directly proportional to the total X-ray luminosity for several orders of magnitude in mass and luminosity (from poor groups to rich clusters). These results point in the direction that data from both parts of the spectrum can uniquely characterise the dynamical state of a cluster.

### 4.1 Isodensity maps

We plot in Figure 2 the smooth APM galaxy distribution as greyscale maps and the X-ray data as isophote contour maps. The three X-ray contours correspond to the density thresholds defined in section 3.2. As expected, clusters in the X-ray appear to be more con-







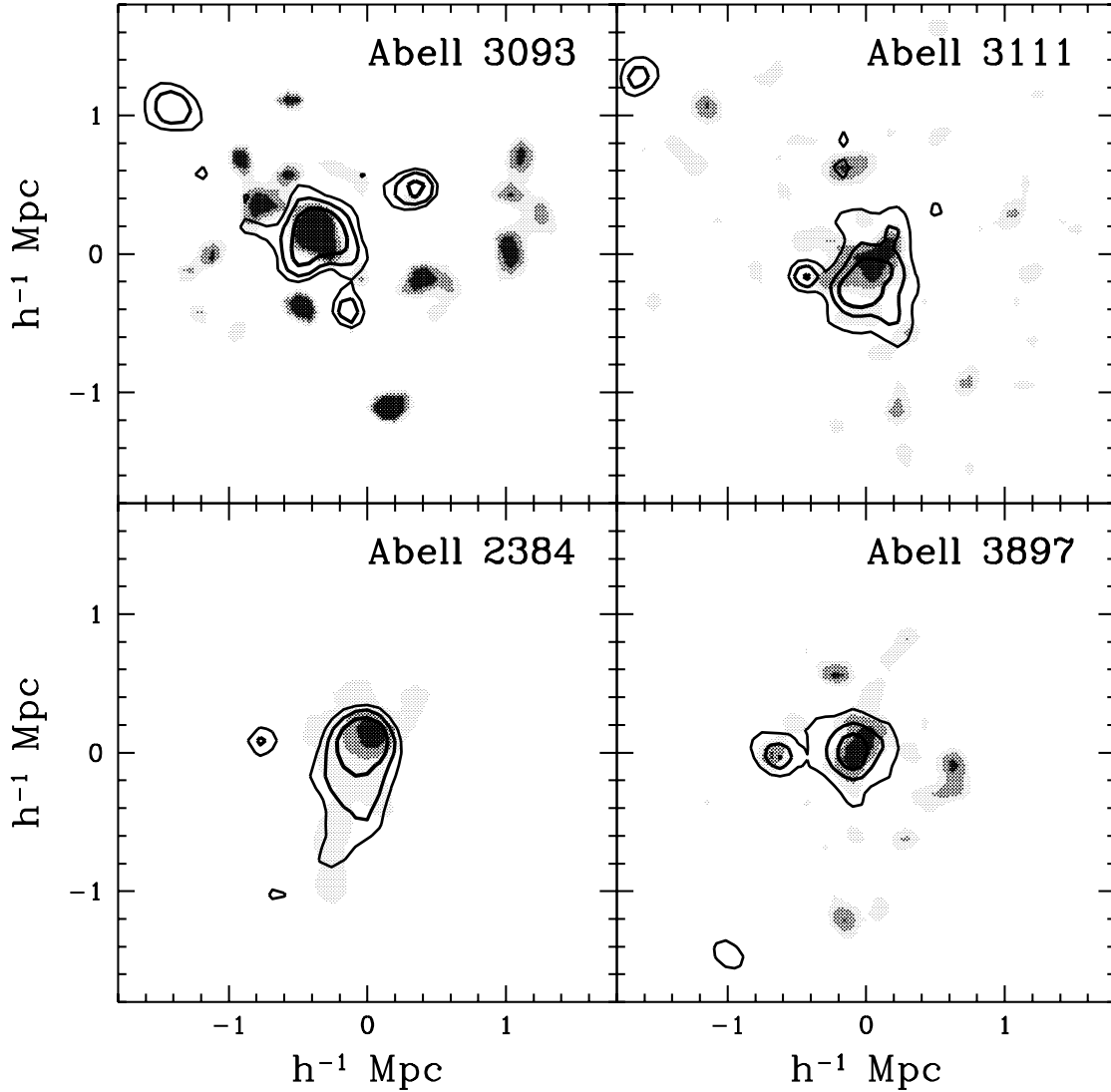


**Figure 2.** Optical and X-ray images for our 22 galaxy clusters. Contours correspond to the X-ray images, whereas greyscale configurations denote the optical data. All axes are expressed in physical units, while the scale of each image is  $\sim 3.6 h^{-1}$  Mpc aside. North is top and East is right.

centrated around the central potential wells, thus having rounder contours than their optical counterparts. Instead, optical data depict more distinct structure (in the form of groups of galaxies) around the core, although this could in some cases, be due to projection effects. A careful comparison with the X-ray maps shows that a few of the clusters in the optical may suffer from such problems, although in some cases galaxy groups, visible only in the optical, may be weak X-ray emitters and hence absent from the X-ray images. Nevertheless, the majority of our clusters seem to have a nice agreement in both parts of the spectrum. In 17 out of 22 systems, the gross features (double and secondary components, elliptical structures, multimodal objects and single, relaxed configurations) of the mass distribution are apparent

in both images. This is an indication that galaxies and groups of galaxies do trace the hot gas distribution in most of the cases ( $\sim 80\%$ ). In only five systems (A2717, A3112, A3897, A3093, A3921), we observe significant apparent substructure in the optical which is (almost) undetectable in the X-rays.

In some of the 17 clusters, with relatively good optical and X-ray image correspondence, there is evidence of recent merger events. Zabludoff & Zaritsky (1995) and Baier et al. (1996) suggest that a substantial spatial difference between the optical and the X-ray peak positions together with the X-ray peak being distorted in an orthogonal direction with respect to the line connecting the two main optical cluster clumps, signify two undeniable collision vestiges. The reason is

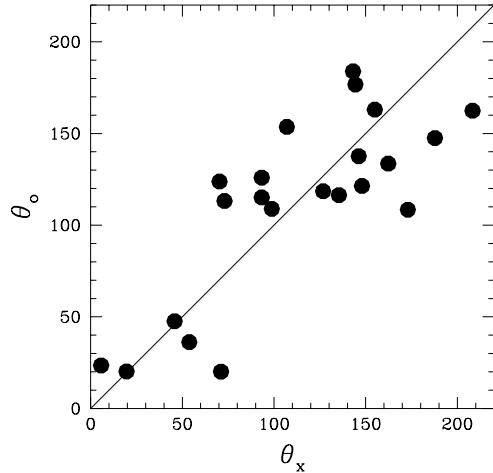


**Figure 3.** Comparison of the X-ray (ROSAT) and optically (APM) defined cluster position angles. The open symbols correspond to the three clusters that have discordant position angles (see text). The solid line corresponds to a perfect correlation.

that gas, unlike galaxies and DM, is collisional. This has been born out also from simulations (Evrard 1990; Roettiger et al 1993) which have shown that during the collision of two groups, the gas is stripped and remains in dis-equilibrium for  $\sim 1 h^{-1}$  Gyr afterwards. Therefore, the criterion of a spatial displacement between the optical and X-ray peak positions seems to be particularly sensitive to the value of  $\Omega_o$ , since it overcomes the known uncertainty of the cluster relaxation time which hampers the cosmological interpretation of the existence of cluster substructure. Such indications, with varying strength, are apparent in A3128, A2804, A3223 and A500 where the corresponding differences between optical and X-ray cluster peaks ( $dp$ ) are of order  $\sim 0.42 h^{-1}$  Mpc,  $\sim 0.58 h^{-1}$  Mpc,  $\sim 0.62 h^{-1}$  Mpc and  $\sim 0.3 h^{-1}$  Mpc respectively. The argument of orthogonality suits best A3128 as is further evident from the large misalignment angles at all  $\rho_t$ 's between the optical and the X-ray mass distributions.

#### 4.2 Position angles

As a first quantitative test of the compatibility between the X-ray and optical images we correlate in Figure 3 their respective cluster major axis orientations. It is evident that there is a good correlation, with coefficient  $\sim 0.8$  and probability of no correlation  $\mathcal{P} \simeq 10^{-5}$ . No cluster has  $\delta\theta \gtrsim 60^\circ$ , while the mean misalignment angle between the cluster optical and X-ray defined position angles is  $\langle \delta\theta \rangle \lesssim 28^\circ \pm 18^\circ$ . Excluding the five clusters that we have identified as having discordant optical and X-ray morphological features we find a similar correlation coefficient but with a slightly lower significance

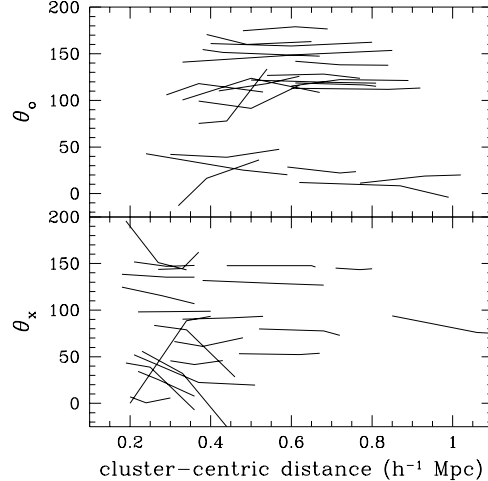


**Figure 4.** Position angle variation as a function of cluster-centric distance for all 22 clusters.

( $\mathcal{P} \simeq 10^{-4}$ ) which is mostly due to the reduction of the sample.

Davis & Mushotzky (1993) have argued that considerable variations of cluster orientations as a function of distance from the cluster center could be considered as evidence of merger events. If, however, subgroups dominantly develop along the filamentary structure in which the cluster is embedded then variations in the cluster position angle could be negligible and thus significant subclumping can escape detection (see West 1995; West et al. 1995). In Figure 4 we examine possible variations in cluster orientations as a function of  $\rho_t$  and thus as a function of distance from the cluster center. For each cluster we connect the position angles estimated at the three density thresholds, and thus at three different distances from the cluster center. It is evident that only a few clusters exhibit evidence for such an effect in their X-ray images, which however should be attributed to their weak position angle determination (due to their extremely small ellipticity).

#### 4.3 Ellipticities

We calculate cluster ellipticities in both data sets as a function of  $\rho_t$ . The cluster  $\epsilon$ 's defined in X-rays are generally slightly smaller than their optical counterparts, corresponding to more spherical configurations (especially for single-component clusters). This is expected when the inter-cluster gas is in hydrostatic equilibrium and the dark matter is distributed like galaxies. However, in the case where we have evidence of recent merger events (A3128, A2804, A3223) we observe that the X-ray ellipticity is typically larger than the corresponding optical. Due to these conflicting trends the correlation between optical and X-ray ellipticities is rather weak as can be seen in Figure 5. Excluding the five sys-

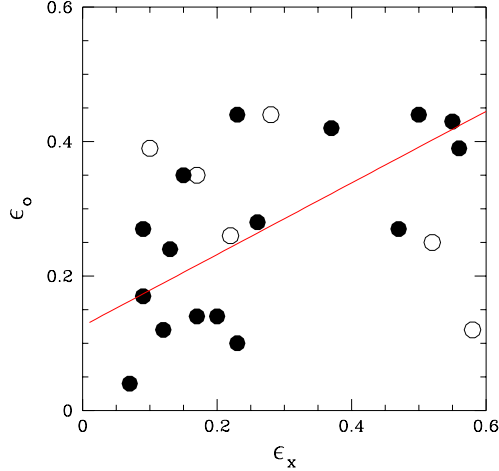


**Figure 5.** Comparison of optical and X-ray defined cluster  $\epsilon$ 's. The 5 clusters with discordant morphologies and A3128 are shown as open circles.

tems with discordant optical and X-ray morphologies (A2717, A3112, A3897, A3093, A3921) and A3128, in which due to a recent merger there is strong differentiation of its X-ray and optical morphology, we find a correlation coefficient of  $\sim 0.7$  with the probability of zero correlation being  $\mathcal{P} \simeq 3 \times 10^{-3}$ .

Another characteristic is that for most clusters (17/22) their optical  $\epsilon$  is a weakly decreasing function of cluster-centric distance, as can be seen in Figure 6, which should be attributed mostly to the effect of background galaxies projected in the area covered by the cluster. In the X-ray images such an effect is evident only in 9 clusters, most of which however are those having large ellipticity. Visual inspection of these clusters show that the effect is not artificial and should be attributed to bimodality at the highest threshold or to the existence of significant substructure located in the central parts of the clusters (cf. A3128, A3223, A2933 etc).

For A2717, A3112, A3897 and A3921 their large  $\epsilon_o$  does not correspond to a similarly large  $\epsilon_x$ , supporting the view that these clusters may suffer from optical projection effects that have altered their true 2D structure (see also section 4.1).

A particularly interesting example is the noisy and apparently highly unrelaxed A3144 cluster. However, its relatively small value of  $\epsilon$  could be possibly attributed to the development of small-scale structures symmetrically around the cluster core or to the existence of significant noise.

## 5 SUBSTRUCTURE RESULTS

We present in this part the results of all the substructure tests that we have applied to the optical and X-ray

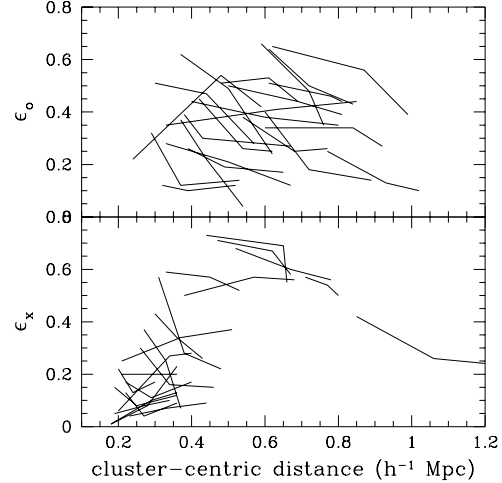


**Figure 6.** Ellipticity variation as a function of cluster-centric distance for all 22 clusters.

cluster data. The results are tabulated in Table 2, together with the cluster shape parameters, discussed in the previous section.

### 5.1 Centroid shifts

We calculate  $sc$ , ie., the difference between the position of the weighted cluster center and the highest density peak as a function of  $\rho_c$  within a radius of  $\sim 0.75 h^{-1}$  Mpc (equation 5). In Figure 7 we correlate the optical and X-ray estimated centroid shifts. We observe a very good correlation between the relative cluster centroid variations for the 17 clusters that have concordant morphological features in both optical and X-rays data (correlation coefficient  $\sim 0.8$  and  $\mathcal{P} \simeq 3 \times 10^{-4}$ ). As expected the significance of the optical  $sc$  (equation 7) is well correlated with the value of the optical and X-ray  $sc$  ( $R \sim 0.9$  and  $\sim 0.8$ , respectively).

*These results indicate that the  $sc$  measure and its significance is a useful tool to characterize the degree of cluster substructure using optical or X-ray data.*

Most of the five clusters that are suspect of being affected by projection effects in the optical (A2717, A3112, A3921) have a large  $sc$  value (only in the optical) and correspondingly high significance indication of subclustering. This fact further suggests that these clusters suffer from projection effects. The cases of A3897 and A3093 are somewhat different, as it is evident from Figure 2. Although there is evidence of projection effects it appears that substructure emerges in a symmetric fashion around the optical cluster core. Such an effect is more pronounced in the optical than in the X-ray images, thus producing as expected a small  $sc$  value.

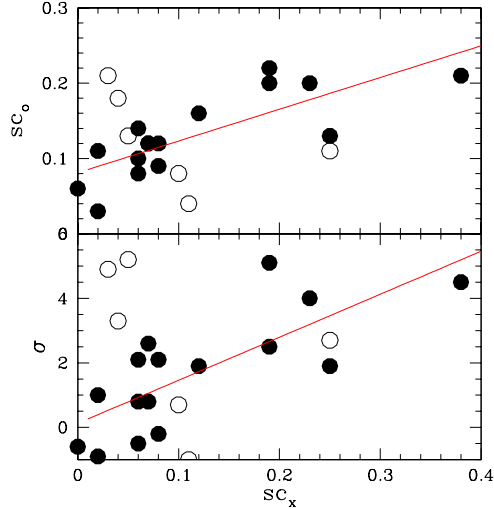


**Figure 7.** Centroid shift statistics. Upper panel: Optical versus X-ray centroid shift values. Lower panel: X-ray  $sc$  values versus optical  $sc$  significance. With open circles we depict the 6 clusters with discordant optical & X-ray morphological features.

## 5.2 Subgroup statistics

Using the categories defined in section 3.3.3 and also a maximum search radius of  $\simeq 0.75 h^{-1}$  Mpc, we obtain 6 clusters falling into the first category of relaxed objects, 6 clusters in the category of systems displaying partial (weak) substructure and 10 clusters belonging to the third case within which clusters exhibit obvious and concrete indications of subclumping events. Note that 4 clusters of the strong substructure case are the ones affected by projections (A3093, A3112, A3897, A3921). In the last column of Table 2 we show the index corresponding to each cluster subgroup index.

The results of this analysis are in good broad agreement with the other substructure measures ( $\epsilon$ 's and  $sc$ 's), with differences only in a few cases. The vast majority of clusters (19 out of 22) show that their subgroup index does agree, at least qualitatively, with the moments analysis that we have applied in this work (section 3). Nevertheless, in 3 cases (A3266, A3301, A2384) results imply discrepancies between our percolation-like algorithm and the method of moments. On checking the parameter space of both techniques, we have found that while the latter stays firm, the former is extremely sensitive to slight alterations regarding the geometric definition of our classes (section 3.3.3).

In the line of the above arguments, we suggest that it is wise to use these results on an advisory level and not as definite.

## 5.3 Comparison of different substructure test

In Figure 8 we correlate ellipticities and  $sc$ 's for all 22 clusters of our sample. The upper panel corresponds to

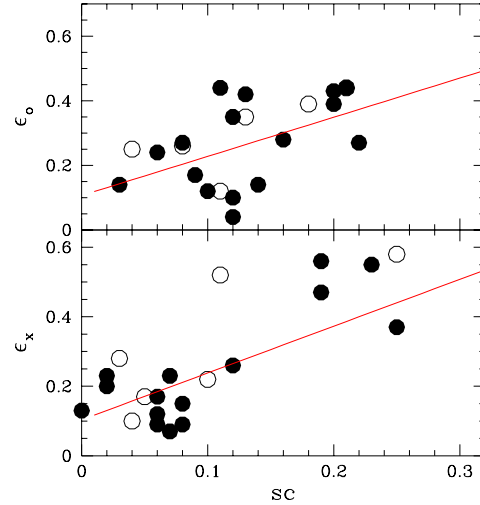


**Figure 8.** Cluster ellipticities as a function of centroid shifts in the optical (top panel) and X-ray (bottom) data, together with the lines of the best fit. Open symbols are as in Figure 7.

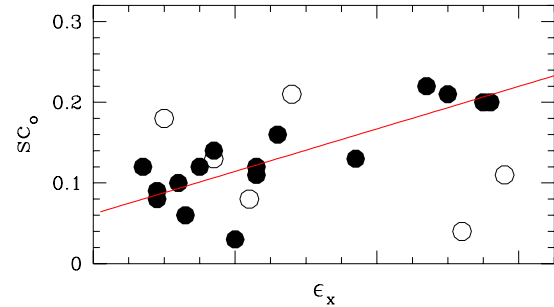


**Figure 9.** Cross-correlation between the cluster X-ray ellipticity and its optical  $sc$  value. Open symbols denote the clusters with discordant optical and X-ray morphological parameters.

the optical and the lower to the X-ray data. It is evident that the two substructure measures are correlated in both sets of data. The correlation coefficients are  $\sim 0.8$  and  $\sim 0.5$  for the X-ray and optical data respectively with probability of zero correlation being  $\mathcal{P} \simeq 10^{-4}$  for the X-ray and  $\mathcal{P} \simeq 0.05$  for the optical data respectively.

Furthermore, cross-correlating, in figure 9, the optical  $sc$ 's and X-ray ellipticities we also find a significant correlation with  $\mathcal{P} \lesssim 10^{-4}$  and  $R \sim 0.82$  if we exclude the clusters with discordant morphologies. We find that the line of best fit is given by:

$$\epsilon_x \simeq 2.55(\pm 0.47)sc_o + 0.07(\pm 0.06) ,$$

from which we can deduce the shape of the ICM region emitting X-rays, directly from optical cluster data.

These results imply that the flattening of clusters, as evident in X-rays as well as in the optical, is a result of their dynamical activity and not due to initial con-

**Table 2.** Results on cluster substructure. Columns 3 to 5 are the  $sc$ ,  $\epsilon$  and  $\theta$  in the X-ray, columns 6 to 8 are the analogous parameters in the optical data, column 9 shows the significance of  $sc_o$ , estimated using equation 7 and column 10 refers to the subgroup category (see section 3.3.3). Note that centroid variations are given in  $h^{-1}$  Mpc and position angles in degrees.

| ACO  | APM | $sc_x$ | $\epsilon_x$ | $\theta_x$ | $sc_o$ | $\epsilon_o$ | $\theta_o$ | $\sigma$ | PG |
|------|-----|--------|--------------|------------|--------|--------------|------------|----------|----|
| 2717 | 5   | .04    | .10          | 143.1      | .18    | .39          | 5.1        | 3.3      | 1  |
| 2734 | 15  | .06    | .09          | 7.8        | .08    | .27          | 147.5      | 0.8      | 2  |
| 2804 | 99  | .19    | .56          | 73.0       | .22    | .27          | 113.2      | 2.5      | 2  |
| 2811 | 104 | .00    | .13          | 135.4      | .06    | .24          | 116.4      | -0.6     | 1  |
| 0133 | 138 | .06    | .12          | 173.2      | .10    | .12          | 108.4      | -0.5     | 2  |
| 2933 | 204 | .23    | .55          | 146.2      | .20    | .43          | 137.6      | 4.0      | 3  |
| 3093 | 347 | .10    | .22          | 70.3       | .08    | .26          | 123.8      | 0.7      | 3  |
| 3111 | 373 | .08    | .15          | 28.3       | .12    | .35          | 162.4      | 2.1      | 2  |
| 3112 | 374 | .05    | .17          | 5.7        | .13    | .35          | 23.5       | 5.2      | 3  |
| 3128 | 403 | .25    | .58          | 53.8       | .11    | .12          | 36.2       | 2.7      | 3  |
| 3144 | 427 | .07    | .23          | 71.1       | .12    | .10          | 20.1       | 2.6      | 3  |
| 3158 | 434 | .06    | .17          | 98.8       | .14    | .14          | 108.9      | 2.1      | 1  |
| 3223 | 484 | .38    | .50          | 144.4      | .21    | .44          | 176.7      | 4.5      | 3  |
| 3266 | 510 | .12    | .26          | 45.8       | .16    | .28          | 47.6       | 2.0      | 1  |
| 0500 | 518 | .07    | .07          | 162.3      | .12    | .04          | 133.6      | 0.8      | 2  |
| 0514 | 533 | .19    | .56          | 126.8      | .20    | .39          | 118.5      | 5.1      | 3  |
| 3301 | 560 | .08    | .09          | 155.2      | .09    | .17          | 163.0      | -.2      | 3  |
| 2384 | 725 | .25    | .37          | 19.6       | .13    | .42          | 20.2       | 2.0      | 1  |
| 3897 | 806 | .11    | .52          | 93.3       | .04    | .25          | 125.9      | -1.0     | 3  |
| 3921 | 822 | .03    | .28          | 93.3       | .21    | .44          | 115.1      | 4.9      | 3  |
| 2580 | 888 | .02    | .23          | 107.0      | .11    | .44          | 153.6      | 1.0      | 1  |
| 4059 | 938 | .02    | .20          | 148.0      | .03    | .14          | 121.4      | -0.9     | 2  |

ditions; for example even high-peaks of an underlying Gaussian random field are aspherical, although less so than lower density peaks (cf. Bardeen et al. 1986).

#### 5.4 Main Results

From the total of 22 clusters, at least in 8 cases we observe strong substructure signatures, verified by all available methods and data (A2804, A2933, A3128, A3144, A3223, A3266, A514, A2384). Of the remaining population we have confirmed, using all our substructure indications, that 9 clusters (A2734, A2811, A133, A3111, A500, A3158, A3301, A2580, A4059) show no or weak substructure activity in both parts of the spectrum (although there is some evidence of a recent merger event in A500). We have also found that 5 clusters (A2717, A3112, A3921, A3093, A3897) appear distinctly bimodal (or even multimodal) although their X-ray contour maps are almost relaxed, which we attribute to projection effects in the optical. From these, A2717, A3112 and A3093 seem to be single-component (relaxed) clusters (based on their X-ray images), while A3921 and A3897 shows clear indications of elliptical systems. Therefore we find that  $\gtrsim 45\%$  of clusters exhibit significant evidence of substructure, which is in good general accordance with most substructure analysis results (see references in Introduction).

Note that out of our 22 clusters, 11 (50%) have been examined for substructure signals elsewhere in the literature (A2717, A133, A3158, A3128, A3266, A500, A514, A2384, A3897, A3921, A4059). We find that our results are in general good qualitative and quantitative agreement with those of other studies (see Appendix). Although, mostly different methods have been employed in these studies (wavelet transform analysis, isophotal maps, power ratios, kinematical and velocity dispersion estimators), we do not detect any serious disparities regarding the dynamical and shape parameters for these X-ray clusters that we have in common. For example we find our position angles always within  $\approx 10^\circ$  of the other determinations.

#### 5.5 Morphological and dynamical classification

We can now proceed in classifying the present sample according to a scheme that is close to the one developed by JF99 (see also Forman & Jones 1990; Jones & Forman 1992; Forman & Jones 1994 and Girardi et al. 1997 hereafter G97). Just to be consistent with the largest and most complete of the above analyses (JF99), we will restrict ourselves only to the X-ray cluster images, which we regard as more reliable in terms of the current assessment (see Table 3).

Clusters with no or marginal evidence of subclumping events are dubbed as single, relaxed objects and given the symbol U, featuring unimodality. In this category we count 12 X-ray clusters. Looking at the strong substructure cases, we have 3 bimodal (B) objects (A2804, A2933 and A3128) out of which the first two show their respective optical doubles, while optical A3128 appears to be somewhat closer to a complex system. We characterise complex or multimodal (M) systems that display more than two clumps in their contour maps. Typical such examples are A3144, A3223 and A514, also authenticated by inspection in the optical. Objects showing apparent deviations from singularity also having large  $\epsilon$ 's, without depicting obvious small-scale structures, are flagged as elliptical (A3266, A2384 and A3921). The latter three clusters, in absence of any other substructure characteristic, are tagged as E's. Finally, A3897 is tagged as P, characteristic of a large central region (primary component) associated with a small secondary structure (left of the X-ray image), visible in both data. Note here, that its optical counterpart would have been flagged as complex, since it shows two extra small-scale clumps at the top and right of the contour plot (see Figure 2).

## 6 CONCLUDING REMARKS

We have investigated a sample of 22 galaxy clusters using optical (APM) and X-ray (ROSAT) data with the

**Table 3.** Codification of our sample according to a modified JF99 classification scheme. The first column denotes the type of activity, second shows the number of clusters falling into that category, third presents its respective fraction to be compared with JF99 results in column 4. Note that the maximum scale of detecting cluster substructure in JF99 is  $0.5 h^{-1}$  Mpc, so that the following comparison should be seen with caution.

| Class | Number | Fraction | JF99  |
|-------|--------|----------|-------|
| U     | 12     | 0.550    | 0.560 |
| B     | 3      | 0.135    | 0.060 |
| M     | 3      | 0.135    | 0.130 |
| E     | 3      | 0.135    | 0.140 |
| P     | 1      | 0.045    | 0.030 |

aim of addressing two questions: (a) Do optical and X-ray data reveal the same cluster morphological features? (b) What is the percentage of relaxed and dynamically active clusters?

Our cluster sample has flown from a cross-correlation between the APM, ACO and ROSAT pointed observations data and has a depth distribution with  $z \lesssim 0.13$ . We have examined our cluster sample utilising several cluster-morphology diagnostics such as isodensity maps, orientations, ellipticities, centroid variations and subgroup statistics. Looking at the isodensity contour maps, the cluster orientations and ellipticities, we observe a remarkable 1-to-1 correspondence between X-ray and optical data in  $\sim 80\%$  of our sample, regarding the gross cluster characteristics (prime structures, elongations, multimodality, collision signatures). We quantify this by correlating the optical and X-ray cluster ellipticities and orientations and find high and statistically significant correlations. In an attempt to quantify the compatibility of the different substructure measures, that we have used, we correlate  $e$ 's and  $sc$ 's, in the optical and in the X-ray separately and we also cross-correlate them to find significant and strong correlations. This implies that indeed the flattening of clusters is due to their dynamical activity.

From our substructure analysis we find that  $\sim 10$  out of 22 systems ( $\sim 45\%$ ) display strong substructure indications visible in both parts of the spectrum. We also find that 5 clusters ( $\sim 22\%$ ) show clear disparities between the optical and X-ray maps, with apparent substructure in the optical not corroborated by the available X-ray data. This is most possibly due to optical projection effects. Our results on the frequency of disordered clusters do concur with most of the relevant studies published to-date.

On the understanding that our catalogue is rather inadequate for drawing significant cosmological conclusions, we would prefer to be cautious when it comes to such a precarious task. Nevertheless, we observe that our present analysis is compatible with that of RLT92 (see their Figure 2) regarding the cluster substructure frequency, setting a rather frail lower limit on

the density parameter ( $\Omega_0 \geq 0.5$ ; see also West 1995; West et al. 1995). Furthermore, the relatively large fraction (4/22) of recent mergers that we have identified is again indicative of a high- $\Omega_0$  Universe (see discussion of Zabludoff & Zaritsky 1995).

In the near future we plan to apply the methodology of this work to  $\sim 900$  APM galaxy clusters, in order to investigate in more detail the issue of cluster substructure.

## ACKNOWLEDGEMENTS

Both S. Basilakos and V. Kolokotronis acknowledge financial support from the Greek State Fellowship Foundation. M. Plionis acknowledges the hospitality of the Astrophysics Group of Imperial College, where this work was completed. This research work has made use of NASA Extragalactic Database (NED). The cluster data have been obtained through LEDAS online service, provided by the University of Leicester.

## REFERENCES

- Abell G., Corwin H., Olowin R., 1989, ApJS, 70, 1  
 Baier F. W., Gastao B. Lima Neto, Whipper H., 1996, in Mapping Measuring and Modelling the Universe (ASP Conference Series Vol. 94), eds. Coles P., Martinez V. J., Pons-Borderia M.-J., Valencia, Spain, 18-22 September, p. 215  
 Bardeen J. M., Bond J. R., Kaiser N., Szalay A. S., ApJ, 304, 15  
 Basilakos S., Plionis M., Maddox S. J., 2000, MNRAS, 315, 779  
 Bird C., 1994, AJ, 107, 1637  
 Bliton M., Rizza E., Burns J. O., Owen F. N., Ledlow M. J., 1998, MNRAS, 301, 3  
 Böhringer H., 1995, in Proceedings of the 17th Texas Symposium on Relativistic Astrophysics and Cosmology, eds. Böhringer H., Trümper J., Morfill G. E., The New York Academy of Sciences  
 Buote D., 1998, MNRAS, 293, 381  
 Buote D., Tsai J., 1995, MNRAS, 452, 522  
 Buote D., Tsai J., 1996, MNRAS, 458, 27  
 Carter D., Metcalfe J., 1980, MNRAS, 191, 325  
 Collins C., Guzzo L., Nichol R., Lumsden S., 1995, MNRAS, 274, 1071  
 Crone M., Evrard A. E., Richstone D., 1996, ApJ, 467, 489  
 Dalton G. B., Croft R., Efstathiou G., Sutherland W., Maddox S., Davis M., 1994, MNRAS, 271, L47  
 Dalton G. B., Maddox S. J., Sutherland W. J., Efstathiou G., 1997, MNRAS, 289, 263  
 Davis D., Mushotzky R., 1993, AJ, 105, 409  
 de Grandi S., Molendi S., 1999, AJ, in press, astro-ph/9910413  
 Dutta S., 1995, MNRAS, 276, 1109  
 Dressler A., Shectman S. A., 1988, AJ, 95, 985  
 Evrard A.E., 1990, in Clusters of Galaxies (STScI Symposium 4), eds. Oegerle W.R. Fitchett M.J., Danly L., Cambridge University Press, p. 287

Evrard A.E., Mohr J.J., Fabricant D.G., Geller M.J., 1993, *ApJ*, 419, L9

Forman W., Bechtold J., Blair W., Giacconi R., van Speybroeck L., Jones C., 1981, *ApJ*, 243, L133

Forman W., Jones C., 1990, in *Clusters of Galaxies (STScI Symposium 4)*, eds. Oegerle W. R. Fitchett M. J., Danly L., Cambridge University Press, p. 257

Forman W., Jones C., 1994, in *Cosmological Aspects of X-ray Clusters of Galaxies (NATO ASI Vol. 441)*, ed. Seitter W. C., Dordrecht: Kluwer, p. 39

Geller M. J., Beers T. C., 1982, *PASP*, 92, 421

Girardi M., Biviano A., Giuricin G., Mardirossian F., Mezzetti M., 1995, *ApJ*, 438, 527

Girardi M., Escalera E., Fadda D., Giuricin G., Mardirossian F., Mezzetti, M., 1997, *ApJ*, 482, 41

Girardi M., Giuricin G., Mardirossian F., Mezzetti M., Boschin W., 1998, *ApJ*, 505, 74

Gomez P. L., Pinkney J., Burns J. O., Wang Q., Owen F. N., Voges W., 1997, *ApJ*, 474, 580

Jones C., Forman W., 1992, in *Clusters and Superclusters of Galaxies (NATO ASI Vol. 366)*, ed. Fabian A. C., Dordrecht: Kluwer, p. 49

Jones C., Forman W., 1999, *ApJ*, 511, 65

Katgert P. et al., 1996, *A&A*, 310, 8

Kriessler J. R., Beers T. C., 1997, *AJ*, 113, 80

Lacey C., Cole S., 1993, *MNRAS*, 262, 627

Lazzati D., Campana S., Rosati P., Chincarini G., Giacconi R., 1998, *A&A*, 331, 41

Mazure A. et al., 1996, *A&A*, 310, 31

McMillan S. L. W., Kowalski M. P., Ulmer M. P., 1989, *ApJS*, 70, 723

Miller, C.J., Melott, A.L., Nichol, R.C., 2000, *ApJ*, *in press*, astro-ph/9912362

Mohr J. J., Fabricant D. G., Geller M. J., 1993, *ApJ*, 413, 492

Mohr J. J., Evrard A. E., Fabricant D. G., Geller M. J., 1995, *ApJ*, 447, 8

Pfeffermann E., Briel U. G., 1986, *SPIE*, 597, 208

Pinkney J., Roettinger K., Burns J., Bird C., 1996, *ApJS*, 104, 1

Plionis M., Barrow J. D., Frenk C. S., 1991, *MNRAS*, 249, 662

Rhee G., van Haarlem M. P., Katgert P., 1991, *A&A*, 246, 301

Richstone D., Loeb A., Turner E. L., 1992, *ApJ*, 393, 477

Rizza E., Burns J. O., Ledlow M. J., Owen F. N., Voges W., Bliton M., 1998, *MNRAS*, 301, 328

Roettiger, K., Burns, J. & Loken, C., 1993, *ApJ*, 407, L53

Sarazin C. L., 1988, *X-ray Emission from Clusters of Galaxies*, Cambridge Astrophysics Series, Cambridge University Press

Schindler S., 1998, in *3rd INTEGRAL Workshop (The Extreme Universe)*, Taormina, Italy, 14-18 September, astro-ph/9811470

Schindler S., 1999, in *Giovanelli F., Sabau-Graziati L., eds., Multifrequency Behaviour of High Energy Cosmic Sources*, Vulcano Workshop 1999, in press, astro-ph/9909042

Serna A., Gerbal D., 1996, *A&A*, 309, 65

Slezak E., Durret F., Gerbal D., 1994, *AJ*, 108, 1996

Solanes J. M., Salvador-Sole E., Gonzalez-Casado G., 1999, *A&A*, 343, 733

Thomas P. A. et al., 1998, *MNRAS*, 296, 1061

Trümper J., 1983, *Adv. Space Sci.*, 2, 241

Valdarnini R., Ghizzardi S., Bonometto S., 1999, *New Astronomy*, 4, 71

West M. J., 1995, in *Clusters of Galaxies (Proceedings of the 29th Recontres de Moriond)*, eds. Durret F., Mazure A., Trân Thanh Vân J., Gif sur Yvette: Frontier Editions, p. 23

West M. J., Bothun G. D., 1990, *ApJ*, 350, 36

West M. J., Jones C., Forman W., 1995, *ApJ*, 451, L5

White D. A., Jones C., Forman W., 1997, *MNRAS*, 292, 419

Zabludoff A., Zaritsky D., 1995, *ApJ*, 447, L21

## APPENDIX A: DETAILS ON INDIVIDUAL CLUSTERS

**A2717:** Obvious similarity of the primary cluster peak ( $\leq 0.4 h^{-1}$  Mpc) but disparity on the secondary structure which is only distinct in the optical image. Suspect of being affected by projection effects. Eight X-ray and radio sources have been removed due to their point-like nature (see also Slezak et al. 1994; Mohr et al. 1995; BT96; G97).

**A2734:** Apparently good correspondence between the two images. Two radio point-like sources (center and upper left) have been subtracted from the X-ray image.

**A2804:** Highly elongated cluster with large and significant *sc*'s in both images. Collision signature visible since the primary optical cluster structure seems to be displaced with respect to its X-ray analogue by  $0.58 h^{-1}$  Mpc. Two radio point-like sources have been excised from the X-ray image.

**A2811:** A relaxed single-component system corroborated by both data, typical of a unimodal configuration. No sources have been removed here.

**A133:** Probably a confirmed unimodal cluster by all substructure measures (Mohr et al. 1995; BT96) showing small values of ellipticities and *sc*'s. Optical and X-ray  $\theta$ 's differ by more than  $64^\circ$ . One projected X-ray source at  $z \sim 0.235$  has been subtracted (EXO 0059.8-2218).

**A2933:** This is the archetype of a bimodal cluster as computed by both data. Highly significant *sc*'s, large ellipticities ( $\simeq 0.5$ ) and similar  $\theta$ 's granting excellent 1-to-1 correspondence. One point-like source has been removed from the upper right of the X-ray image.

**A3093:** Four point-like sources have been excised from the X-ray data (center bottom and left). This system has mediocre ellipticities and non-significant centroid shifts. It also yields a  $\delta\theta \simeq 54^\circ$ . Suspect of being affected by projection effects.

**A3111:** Partial substructure activity present at very low density thresholds. If taken at face value, system would have been flagged as complex. Isodensity contour plots are very similar, whereas its respective  $\delta\theta$  is more than  $45^\circ$ . Like the previous one and in the absence of any distinct activity, it is regarded as a relaxed object.

Five point-like sources have been removed from the X-ray cluster map.

**A3112:** No sources were subtracted here. This is the archetype of image disparity. Obvious bimodality in the optical (a  $5.2\sigma$  *sc* event) corresponds to definite unimodality in the X-rays. Excluded from the cross-correlation statistical analysis (together with A2717, A3897, A3921 and A3093) as being suspect of optical projections.

**A3128:** One radio point-like source (PMN: JO331-S242) has been removed (lower right of X-ray map). Dissimilar cluster orientations and ellipticities are typical of a collision event between the prime cluster structures. Despite that, it exhibits highly significant *sc*'s ( $\sim 3\sigma$ ) in both data. In the G97 analysis this cluster is dubbed as a unimodal object on a scale of  $\sim 1 h^{-1}$  Mpc. Notice that the latter study is based on an entirely different approach than the one developed here.

**A3144:** This is a typical complex system. Multiple peaks associated with marginally significant *sc*'s and medium  $\epsilon$ 's due to symmetrically developed structures around the central cluster potential wells. No sources have been excluded here.

**A3158:** A single-component cluster, well-aligned and also showing small values of ellipticities and insignificant *sc*'s (Slezak et al. 1994; Mohr et al. 1995; BT96; G97). The optical *sc*  $\sim 0.14 h^{-1}$  Mpc is only a  $2\sigma$  substructure event. No sources have been removed.

**A3223:** Typical complex system displaying large  $\epsilon \simeq 0.5$  and the largest *sc*  $\sim 0.38 h^{-1}$  Mpc out of the whole sample. Optical peak appears to be largely displaced with respect to the X-ray one ( $dp \sim 0.62 h^{-1}$  Mpc), a fact that signifies a collision vestige. Four radio point-like sources have been subtracted from the X-ray map (upper left, right and lower left).

**A3266:** We have classified this cluster as elliptical in the absence of other distinct features. Optical and X-ray images are well-aligned. No sources excised (see also Mohr et al. 1993; 1995; BT96; G97; de Grandi & Molendi 1999).

**A500:** Good correspondence between optical and X-ray isodensity maps. It shows weak substructure which is rather insignificant. However, there are indications of a possible recent merger (displacement of optical and X-ray peaks by  $dp \leq 0.3 h^{-1}$  Mpc). No sources have been removed from the X-ray map. Similar studies (Mohr et al. 1995; BT96) show evidence of a unimodal cluster at least within  $\sim 0.5 h^{-1}$  Mpc in all substructure properties.

**A514:** Another classical multimodal system with distinct density peaks in both maps. Large ellipticities are followed by analogously large and statistically significant *sc*'s ( $\sim 5\sigma$ ). Two X-ray and two radio point-like sources have been omitted here. This is the complex archetype in most of the published works up till now

(see also West et al. 1995; BT96; Bliton et al. 1998; JF99).

**A3301:** Two point-like sources have been subtracted from the left of the X-ray map. Definitely unimodal in the X-ray but slightly elongated and multimodal in the optical, although with an insignificant *sc*. Relatively good 1-to-1 correspondence of the contour maps.

**A2384:** This is the archetype of an elliptical cluster. A high quality HRI image ( $t_{\text{exp}} > 7$  hrs) which exhibits large *sc*'s and  $\epsilon$ 's in both images. However, the *sc* values are marginally significant. No sources have been removed in this case (see also McMillan et al. 1989; West et al. 1995).

**A3897:** An object with distinct substructure in both data, typical of the category P (see X-ray map). Notwithstanding that, it seems multimodal in the optical. The optical *sc* is non-significant but it is apparent that it is somehow underestimated due to symmetric and equally-sized structures developing around the central core. The same reasoning fully explains the low  $\epsilon_0$ . Suspect of being affected by projection effects. Three point-like sources have been excised at the lower left of the X-ray image (see also Gomez et al. 1997).

**A3921:** A definitely optically complex object which is seemingly unimodal in the X-rays. There are, however, traces of elongation in the X-ray contour plot, only at the lower  $\rho_t$ . This extension appears to be in the exact direction of the secondary optical structure which is not visible in the X-ray map. As a result, both data maps seem to be well-aligned and we have therefore classified A3921 as an elliptical object but we have also considered it as being affected by projection effects in the optical. Three point-like sources (center and lower left) have been removed from the X-ray cluster (see also Mohr et al. 1995; BT96).

**A2580:** Within  $0.5 h^{-1}$  Mpc of the highest cluster peak, this cluster seems relaxed and unimodal in both images. There is some substructure evidence by means of the optical *sc* (non-significant) and ellipticity, while it appears slightly misaligned ( $\delta\theta \leq 47^\circ$ ). No sources have been subtracted from this system.

**A4059:** This is another typical unimodal system. A low *sc* object which displays remarkable accordance in the isodensity maps and a  $\delta\theta \leq 27^\circ$ . No sources have been removed from this one. Definitely dubbed as a single-component cluster also by other analyses (cf. Slezak et al. 1994; Mohr et al. 1995; BT96; G97).

